Some Experiments with Mosaic Models for Images

NARENDRA AHUJA, TSVI DUBITZKI, AND AZRIEL ROSENFELD, FELLOW, IEEE

Abstract—**Experimental results are presented on some properties of random mosaic models for textures. These observations are compared with the theoretically predicted values. The predictions are also compared with observations on a real image.**

I. Introduction

SEVERAL geometric and joint pixel properties of the patterns generated by mosaic models were studied in [1], [2]. Among the geometric properties the theoretical results obtained for the expected component perimeter and expected component width for the cell structure models were not verified experimentally. Also, no experiments involving real textures were reported.

While the component perimeter and width results for the regular cell structure models [1], [2] are fairly straightforward, the results for random cell structure models may warrant experimental verification to justify the validity of the assumptions made in deriving them. This paper compares the theoretically predicted values of the expected component area and perimeter with the corresponding observed values on patterns generated by the models. Some results are also presented on how the predictions of the models relate to observations on a real image.

Section II reviews the three random mosaic models that we considered for the experiments reported in this paper. Section III briefly outlines the analytical results for the expected component perimeter and contrasts them with the observations. Section IV presents similar results for the expected component width. Section V presents some concluding remarks.

II. Random Cell Structure Mosaic Models

Cell structure mosaics are constructed in two steps: 1) tessellate a planar region into cells (we will only consider tessellations composed of bounded convex polygons), and 2) independently assign one of m colors $c_1, c_2, \cdots, c_m$ to each cell according to a fixed set of probabilities

$$p_1, \cdots, p_m; \quad \sum_{i=1}^{m} p_i = 1.$$

The set of colors may correspond to a set of values of any property, not necessarily gray level.

Different types of tessellations provide different types of mosaics. This paper considers three models that use three random tessellations of the plane. These models and some properties of the tessellations they use are described below (for details see [1], [8], [9]; also see [6]).

A. Poisson Line Model

Consider a system of intersecting lines in the plane with random positions and orientations. Such a system when derived by the following Poisson process possesses fundamental properties of homogeneity and isotropy. A Poisson process of intensity λ/π determines points (θ, p) in the infinite rectangular strip $[0 \leqslant \theta < \pi, -\infty < p < \infty]$. Each of these points can be used to construct a line in the plane of the form $x\cos\theta + y\sin\theta - p = 0$, where p is the distance to an arbitrarily chosen origin. One can use this process to tessellate any finite region into convex cells having the following properties:

$E(A) \equiv$ expected cell area $= \pi/\lambda^2$;
$E(S) \equiv$ expected cell perimeter $= 2/\lambda$;
$E(N) \equiv$ expected number of sides of a cell $= 4$.

B. Occupancy Model

This model is based upon a tessellation that is the result of a growth process. A Poisson process of intensity λ drops nuclei in the plane. Each of these points spreads out to occupy a "Voronoi cell" consisting of all the points which are nearer to it than to any other nucleus. The random initial arrangement of the nuclei results in cell edges with infinitely many slopes and, therefore, a random tessellation. The cells are convex having the following properties:

$$E(A) = \frac{1}{\lambda}$$

$$E(S) = \frac{4}{\sqrt{\lambda}}$$

$$E(N) = 6.$$

Manuscript received June 4, 1979; revised January 18, 1980 and July 17, 1980. This work was supported by the Defense Advanced Research Projects Agency and the U.S. Army Night Vision Laboratory under Contract DAAG-53-76C-0138 (DARPA Order 3206)

N. Ahuja was with the Computer Vision Laboratory, Computer Science Center, University of Maryland, College Park, MD. He is now with the Coordinated Science Laboratory and Department of Electrical Engineering, University of Illinois, Urbana, IL 61801

T. Dubitzki and A. Rosenfeld are with the Computer Vision Laboratory, Computer Science Center, University of Maryland, College Park, MD 20742.

0018-9472/80/1100-0744$00.75

C. Delaunay Model

The Delaunay tessellation is closely related to the occupancy model. It can be constructed from the occupancy tessellation by joining, for each vertex of the Voronoi tessillation, all pairs of nuclei whose cells meet at the given vertex and share a common edge. Thus the intersections of the borders of Voronoi cells are the circumcenters of the Delaunay cells. These cells have the following properties:

$$E(A)=\frac{1}{2\lambda}$$

$$E(S)=\frac{32}{3\pi\sqrt{\lambda}}$$

$$E(N)=3.$$

III. Expected Perimeter

We first briefly review computation of the expected perimeter for connected components in the random mosaics. Details can be found in [1], [2]. Then we evaluate the expressions obtained for the expected perimeter and compare these predicted values against observations on several images.

A. Theoretical Computation

We will obtain the expression for the expected perimeter of a black component in a binary (black and white) mosaic for easy description, although the results also hold for components of multicolored mosaics. Let p and $1-p$ denote the probability that an arbitrary cell is black or white, respectively. Then the expected number of white cells neighboring a black cell is $(1-p)E(N)$, where $E(N)$ is the expected number of neighbors in a cell in the tessellation. The expected number K of cells in a black component for a given p is also known [1], [2]. Therefore, we have

$$\text{expected number of cell edges along the border of a component} = K(1-p)E(N).$$

Since $E(N)$ is also the expected number of cell edges along a cell border, we have

$$\begin{aligned} H &\equiv \text{expected perimeter of a component} \\ &= K(1-p)\ \text{(expected cell perimeter)} \\ &= K(1-p)E(S). \end{aligned}$$

Substituting from Section II the expressions for $E(S)$ for the various models, we obtain the following expressions for the expected perimeter.

Poisson line model:

$$H=K(1-p)\frac{2}{\lambda};$$

occupancy model:

$$H=K(1-p)\frac{4}{\sqrt{\lambda}};$$

Delaunay model:

$$H=K(1-p)\frac{32}{3\pi\sqrt{\lambda}}.$$

Note that K is different for each of the three models.

B. Experimental Results

Results for the occupancy and Delaunay models were tested on two sets of four mosaics each. Occupancy and Delaunay tessellations were generated using Poisson point processes of intensities 0.003 and 0.001, respectively. An interior window (consisting of 100 cells) was used for the purpose of observations in order to avoid border cells that may have different geometrical properties. Figs. 1–4 show the tessellations and the corresponding binary mosaics. The perimeter was measured by following the borders of the components and counting 1 for every horizontal or vertical step and $\sqrt{2}$ for every diagonal step. Table I lists the average total observed perimeter for each of the two sets of mosaics. These values are compared with the predicted total expected perimeter values. The differences are expressed as fractions of the observed values. Note that the total perimeter values that we have listed in the table differ from the component perimeter values by a multiplicative constant equal to the expected number of components, which is known [1], [2].

Generation of Poisson line mosaics on the grid involves certain problems. There is a nonzero probability of a small cell being lost due to the nonzero thickness of digital lines. In other words, a small cell in a Poisson line tessellation in the Euclidean plane may cease to have any pixels in its interior in the digital version. A cell may reduce to a small set of black pixels each belonging to one of the surrounding digital lines. Such cells, if not properly taken care of, may change the connectedness properties of the digital Poisson line mosaics. To avoid this we must use low intensity values. However, this requires working with

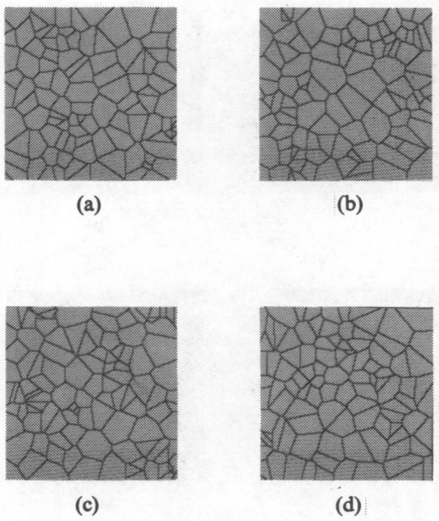

Fig. 1. Occupancy tessellations ($\lambda=0.003$).

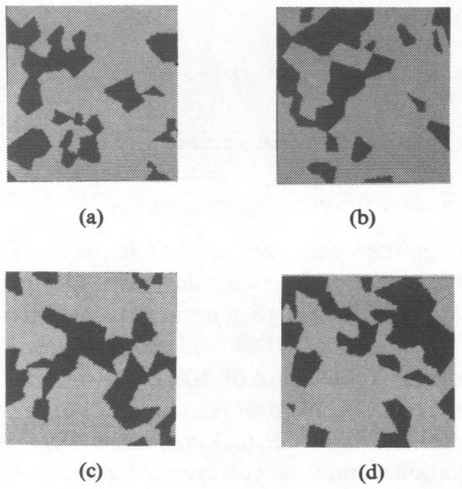

Fig. 2. Occupancy mosiacs (Fig. 1 (a)–(d) colored with $p=0.3$).

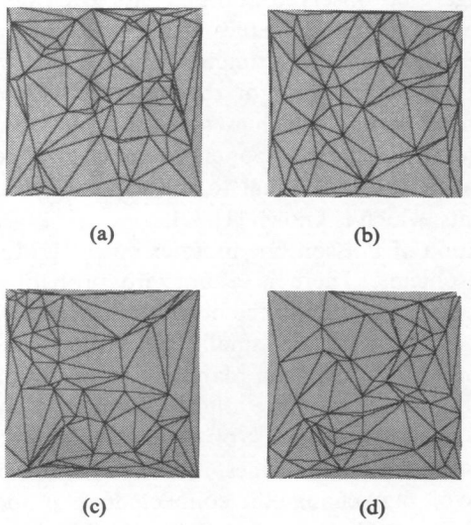

Fig. 3. Delaunay tessellations ($\lambda_0=0.001$).

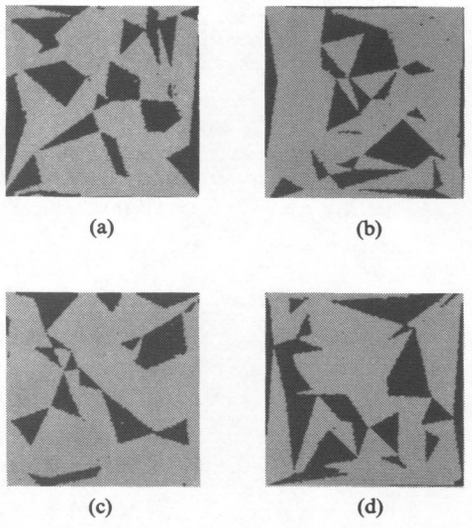

Fig. 4. Delaunay mosiacs (Fig. 3 (a)–(d) colored with $p=0.3$).

TABLE I
EXPECTED PERIMETER RESULTS FOR MOSAICS

Model	Observed average total perimeter on four mosaics (=a)	Predicted expected total perimeter (=b)	% Deviation $= \frac{b-a}{a} \times 100$
Occupancy	1525.5	1567.6	2.7
Delaunay	1666.5	1804.0	8.2

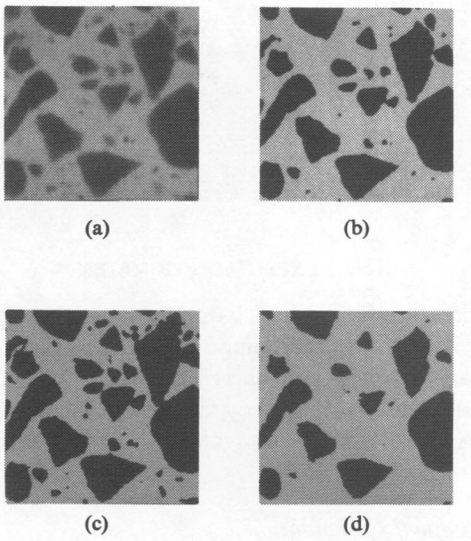

Fig. 5. (a) Marble picture (Plate 62 from [3]). (b)–(d) Same as (a) thresholded at 25, 17, and 36, respectively.

large images in order to have a large number of cells, thus increasing computational costs. We therefore considered only the occupancy and Delaunay mosaics for the perimeter experiments.

We also investigated the predictability of the expected component perimeter in a natural image, treating it as a random cell structure mosaic (Fig. 5(a)). A relatively high contrast image (Brodatz [3, plate D62]) was chosen for the reason of ease in segmentation. The image has a fairly bimodal histogram. A threshold between the two peaks was used to extract the components. The two parameters, λ and p, defining the binary models, were evaluated from the observed average component area and density, using the known nature of dependence of these features on the parameters.

The value of p was estimated from the fraction of the image area occupied by the (black) components. The total observed number of components in the interior of the image and the estimated value of p, in conjunction with the expected component area results [1], [2], provide an estimate of λ. Then the formulas of Section III-A can be used to predict the expected perimeter according to the various models.

Clearly, the values of the image features we are considering are sensitive to the threshold chosen. To test the consistency of the predictions from the same model and the relative performance of the different models for different segmentations, we used three different thresholds cor-

TABLE II
EXPECTED PERIMETER RESULTS FOR MARBLE IMAGE

Threshold	Average	Poisson line model		Occupancy model		Delaunay model	
	Observed total perimeter (=a)	Predicted total perimeter (=b)	% Deviation $=\frac{b-a}{a}\cdot 100$	Predicted total perimeter (=c)	% Deviation $=\frac{c-a}{a}\cdot 100$	Predicted total perimeter (=d)	% Deviation $=\frac{d-a}{a}\cdot 100$
17	2520	3243.0	29.7	8842.0	250.0	5522.0	119.0
25	2013	2695.0	33.8	8250.0	309.0	8055.0	300.0
36	1453	1975.0	35.9	2485.0	71.0	3045.0	109.0

responding to the middle and the two ends of the valley between the histogram peaks. Figs. 5(b)–(d) show the three segmentations. Table II lists the observed and the predicted expected total perimeter for each of the three models and the three thresholds. The differences between the predicted and the observed values are listed as fractions of the observed values. The predictions according to the Poisson line model are consistently better compared to those from the other two models. Also the errors in the Poisson line model predictions appear to be less sensitive to threshold variations.

IV. EXPECTED WIDTH

The expected width of a connected component is defined as the length of the intercept made by a randomly located and oriented line transect. In [1], [2] we analyzed this property for various models. Here we will briefly review these results for the three random cell structure models and then compare these predictions with observed values.

A. Theoretical Computation

Consider the distribution of the variate L_i, the width as measured along a transect, of a component of color c_i. This width is a sum of the widths of one or more contiguous cells that happen to have received the same color c_i.

If there are j contiguous cells in the component along the sampling transect and x denotes the width of a cell, then the desired component width is the sum of j values of x. A given run of length L_i consists of exactly j cells if the first cell is followed by $j-1$ cells of color c_i and if the jth cell is not of color c_i. Thus the probability that a run of color c_i is of length j is $p_i^{j-1}(1-p_i)$. If $g(L_i|j)$ denotes the conditional probability density of the length of a run, given that it consists of j cells, we have

$$g(l_i)=\sum_{j=1}^{\infty} g(l_i|j)p_i^{j-1}(1-p_i).$$

Then the expected value $E(L_i)$ of the run length is given by

$$E(L_i)=\sum_{j=1}^{\infty} E(L_i|j)p_i^{j-1}(1-p_i).$$

We will make the simplifying assumption that the widths of adjacent cells along a given transect are independent. This assumption may not be satisfied by the occupancy model, whose cells are not independent. However, it seems plausible that the correlations involved are not high and the results for relatively large components are satisfactory. The expression for $E(L_i)$ obtained earlier then becomes

$$E(L_i)=\sum_{j=1}^{\infty} E(L_i|j)p_i^{j-1}(1-p_i).$$

From the independence assumption, it follows that

$$E(L_i|j)=jE(L_i|1)=j \text{ (expected cell width)}.$$

Therefore,

$$E(L_i)=(1-p_i)\sum_{j=1}^{\infty} j p_i^{j-1} \text{ (expected cell width)}$$

$$=\frac{1}{1-p_i} \text{ (expected cell width)}.$$

For black components in binary mosaics, we have

$$E(L)=\frac{1}{1-p} \text{ (expected cell width)}.$$

We have not given the distribution of the cell width x for either the occupancy or Delaunay models. However, in one of his classic results Crofton [4] showed that the mean length of a randomly oriented chord of a convex region depends upon the shape of the region only through its area A and perimeter S as follows:

$$\text{mean chord length}=\frac{\pi A}{S}.$$

Since all of our models have convex cells, with known expected area and perimeter, we have

$$\text{expected cell width}=E\left[\frac{\pi A}{S}\right]$$

$$=\pi E\left(\frac{A}{S}\right).$$

$E(A/S)$ is not known for any of our models. However, a fair substitute for $E(A/S)$ is given by $E(A)/E(S)$ [5]. Therefore,

$$E(L_i)=\frac{\pi}{1-p_i}\frac{E(A)}{E(S)}.$$

Using the above relations in conjunction with the expected cell area and expected cell perimeter properties given in Section II, we now obtain specific results for the three random models.

Poisson line model:

$$E(L)=\frac{\pi E(A)}{E(S)(1-p)}=\frac{1}{2\lambda(1-p)}.$$

TABLE III
EXPECTED COMPONENT WIDTH RESULTS FOR MOSAICS

Model	Observed average total perimeter on four mosaics (=a)	Predicted expected total perimeter (=b)	% Deviation $= \frac{b-a}{a} \times 100$
Occupancy	20.00	19.45	2.65
Delaunay	16.31	14.76	10.5

TABLE IV
EXPECTED COMPONENT WIDTH RESULTS FOR MARBLE IMAGE

Threshold	Average	Poisson line model		Occupancy model		Delaunay model	
	Observed component width (=a)	Predicted component width (=b)	% Deviation $= \frac{b-a}{a} \cdot 100$	Predicted component width (=c)	% Deviation $= \frac{c-a}{a} \cdot 100$	Predicted component width (=d)	% Deviation $= \frac{d-a}{a} \cdot 100$
17	21.06	19.27	8.5	7.02	65.8	11.27	46.4
25	20.95	19.07	8.9	11.86	43.3	12.19	42.0
36	21.43	19.14	10.6	15.11	29.4	12.43	42.0

For the Poisson line model we also know the distribution of the length of a random chord of a cell. Therefore, we can also obtain the distribution of the component width in [1], [7]. In fact, the probability density function of the width of a component has the same form as that of the width of a single cell, i.e., exponential. The knowledge of the distribution of the component width is another result of the extreme mathematical tractability of the Poisson line model. The corresponding property is not known for either of the remaining models.

Occupancy model:

$$E(L) = \frac{\pi}{4\sqrt{\lambda}\,(1-p)}.$$

Delaunay model:

$$E(L) = \frac{3\pi^2}{64\sqrt{\lambda}\,(1-p)}.$$

B. Experimental Results

The component size grows rapidly with increasing values of p. If we have large components we need large images for measurement of component properties, in order to have access to a large number of components. Thus the p value must be kept relatively low to work with images of reasonable size. We used a p value of 0.3, as in Section III, and a set of four mosaics each to estimate the average component width in the occupancy and the Delaunay mosaics. Since the expected component width is independent of the direction in which it is measured, we can use run lengths of black points in horizontal (and vertical) directions to estimate the component width. Table III lists the observed average run lengths of black pixels and the predicted expected component widths for the occupancy and the Delaunay models. The deviations normalized by the observed values are also listed. The Poisson line mosaics were not generated for the reasons mentioned in Section III. However, we may note that the results for this model were obtained completely analytically and hence may not have to be verified experimentally. Between the occupancy and the Delaunay models, the predictions made by the former are closer to observations.

The marble image from [3] used in Section III-B was also used to test the width results. The model parameters were evaluated based upon the observed total black area and the total number of components in the interior of the image. The predicted and observed expected width values for the three models and the three different thresholds are given in Table IV. The normalized deviations are also listed. The Poisson line model gives the least error in predicting the average component width, and the error is relatively insensitive to the variations in the threshold value chosen for segmentation.

V. CONCLUSION

We have presented the observed and predicted expected component perimeter and width values for the occupancy and Delaunay models. The error for the Delaunay model is higher than that for the occupancy model for each property. It is hard to assess the significance of these errors since we do not know the probability distributions involved. As pointed out earlier, the results for the Poisson line model were derived analytically and hence may not have to be tested through experiments. On the marble image, the Poisson line model gives consistently lower errors compared to the other two models. The absolute significance of these errors is once again hard to evaluate except, perhaps, for the Poisson line model. This model also exhibits relatively stable performance with varying threshold value used for segmentation.

ACKNOWLEDGMENT

The help of Kathryn Riley in preparing this paper is gratefully acknowledged.

REFERENCES

[1] N. Ahuja, "Mosaic models for image analysis and synthesis," Doctoral dissertation, Dep. Comput. Sci., Univ. of Maryland, College Park, Mar. 1979.

[2] N. Ahuja, "Connectivity in lattices and mosaics," in *Proc. 4th Int. Joint Conf. Pattern Recognition*, pp. 488–493.

[3] P. Brodatz, *Textures: A Photographic Album for Artists and Designers*. New York: Dover, 1966.

[4] M. W. Crofton, "Probability," in *Encyclopedia Britannica*, 9th ed., 1885.

[5] R. E. Miles, "On the homogeneous planar Poisson point process," *Math. Biosci.*, vol 6, pp. 85–127, 1970.

[6] J. W. Modestino, R. W. Fries, and A. L. Vickers, "Stochastic image models generated by random tessellations of the plane," *Computer Graphics Image Processing*, vol., 12, pp. 74–98, 1980.

[7] E. Pielou, *Mathematical Ecology*. New York: Wiley, 1977.

[8] B. Schachter, A. Rosenfeld, and L. Davis, "Random mosaic models for textures," *IEEE Trans. Syst. Man, Cybern.*, vol. SMC-8, pp. 694–702, 1978.

[9] B. Schachter and N. Ahuja, "Random pattern generation processes," *Computer Graphics Image Processing*, vol. 10, pp. 95–114, 1979.

Correspondence

An Energy Use Model of the Residential Sector

DENNIS L. O'NEAL AND ERIC HIRST

Abstract—**A model to simulate energy use in the residential sector from 1970 through 2000 is described. The model provides considerable detail on residential energy uses and associated costs. It estimates annual energy uses for four fuels, eight end uses, and three housing types. Each fuel use component is calculated as a function of stocks of occupied housing units and new construction, average housing size, equipment ownership by fuel and end use, thermal performance of housing units, average unit energy requirements for each equipment type, and usage factors that reflect household behavior. The model also estimates annual equipment installations and ownership, equipment costs, and costs for improving thermal performance of new and existing housing units. The model is a useful tool for evaluating alternative energy conservation policies, programs, and technologies for their energy and economic effects during the next quarter century. An example of its application in estimating the energy and economic impact of alternate water heating conservation options is provided. Results from this application indicate the attractiveness of heat pump water heaters over both conventional and solar heaters. The estimated cumulative energy savings of heat pump and solar heaters (with Federal tax credits) were 1.6 and 1.0 EJ, respectively.**

INTRODUCTION

In 1975, development began at the Oak Ridge National Laboratory (ORNL) of a model of energy use for the residential sector. The initial version of the model was completed in 1976 and has since been improved and expanded [1], [2]. The primary purpose of the modeling effort was to develop an analytical tool which would assist decisionmakers in federal agencies and other organizations in their evaluation of conservation strategies and programs. The model has been used in such diverse applications as evaluating the residential sector programs in the national Energy Plan (NEP) [3], estimating the impact of residential RD&D [4], and evaluating residential energy use trends for the National Academy of Sciences Committee on Nuclear and Alternative Energy Systems (CONAES). Over 20 organizations (both public and private) have used the residential model.

Manuscript received January 14, 1980; revised August 13, 1980. This work was supported by the Energy Information Administration and the Office of Conservation and Solar Applications, U.S. Department of Energy under contract W-7405-eng-26 with the Union Carbide Corporation.

The authors are with the Energy Division, Oak Ridge National Laboratory, Oak Ridge, TN 37830.

ORNL RESIDENTIAL MODEL SENSITIVE TO MAJOR DETERMINANTS OF ENERGY USE

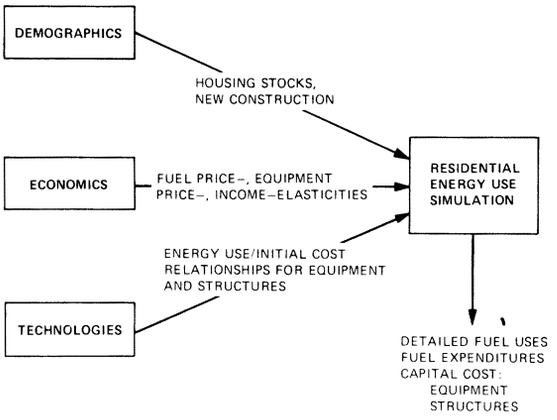

Fig. 1. Schematic, ORNL residential energy use model.

The energy model consists of three kinds of submodels: demographic, technological, and economic (see Fig. 1). The demographics submodel calculates stocks of occupied housing units by type for each year of the simulation based on calculations of household formation and retirements from the existing stock of occupied housing units.

The technologies submodels evaluate changes in energy requirements and purchase price as functions of alternative designs for both equipment (e.g., furnaces, refrigerators, etc.) and the thermal integrity of structures.

The economics submodels calculate elasticities that determine the responsiveness of households to changes in economic variables: incomes, fuel prices, and equipment prices. Elasticities are

0018-9472/80/1100-0749$00.75